frontiers | Frontiers in Physics

ORIGINAL RESEARCH
published: 11 July 2022
doi: 10.3389/fphy.2022.957025

Check for updates

Effects of Branched Fins on Alumina and N-Octadecane Melting Performance Inside Energy Storage System

Wajaree Weera[1]*, Apichit Maneengam[2], Abdulkafi Mohammed Saeed[3,4], Abderrahmane Aissa[5], Kamel Guedri[6], Obai Younis[7], Riadh Marzouki[8,9] and Kanayo K. Asogwa[10]

[1]Department of Mathematics, Faculty of Science, Khon Kaen University, Khon Kaen, Thailand, [2]Department of Mechanical Engineering Technology, College of Industrial Technology, King Mongkut's University of Technology North Bangkok, Bangkok, Thailand, [3]Department of Mathematics, College of Science, Qassim University, Buraydah, Saudi Arabia, [4]Department of Mathematics, College of Education, Hodeidah University, Al-Hudaydah, Yemen, [5]Laboratoire de Physique Quantique de la Matière et Modélisation Mathématique (LPQ3M), University of Mascara, Mascara, Algeria, [6]Mechanical Engineering Department, College of Engineering and Islamic Architecture, Umm Al-Qura University, Mecca, Saudi Arabia, [7]Department of Mechanical Engineering, College of Engineering at Wadi Addwaser, Prince Sattam Bin Abdulaziz University, Wadi Addwaser, Saudi Arabia, [8]Chemistry Department, College of Science, King Khalid University, Abha, Saudi Arabia, [9]Chemistry Department, Faculty of Sciences of Sfax, University of Sfax, Sfax, Tunisia, [10]Department of Mathematics, Nigeria Maritime University, Okerenkoko, Nigeria

OPEN ACCESS

Edited by:
Animasaun I. L., Federal University of Technology, Nigeria

Reviewed by:
Abayomi Samuel Oke, Adekunle Ajasin University, Nigeria
H. A. Kumara Swamy, Presidency University, India
N. Keerthi Reddy, Ulsan National Institute of Science and Technology, South Korea

***Correspondence:**
Wajaree Weera
wajawe@kku.ac.th

Specialty section:
This article was submitted to Interdisciplinary Physics, a section of the journal Frontiers in Physics

Received: 30 May 2022
Accepted: 20 June 2022
Published: 11 July 2022

Citation:
Weera W, Maneengam A, Saeed AM, Aissa A, Guedri K, Younis O, Marzouki R and Asogwa KK (2022) Effects of Branched Fins on Alumina and N-Octadecane Melting Performance Inside Energy Storage System. Front. Phys. 10:957025. doi: 10.3389/fphy.2022.957025

The importance of Phase change material (PCM) energy storage systems is no longer new in the industry. However, the influence of using branched fins inside the energy storage system on the melting process of alumina nanoparticles and n-octadecane has not been reported in the literature. Consequently, the outcome of a study on the numerical simulation for optimizing the melting performance of a PCM in various tubes, including those with branching fins is presented in this report. Four examples were assessed in relation to a suspension of alumina nanoparticles and n-octadecane paraffin that contains heated fins. A numerical technique based on the Galerkin finite element method (GFEM) was used to solve the dimensionless governing system. The average liquid percentage over the flow zone in question was computed. The primary results indicated that altering the number of heated fins might affect the flow structures, the system's irreversibility, and the melting process. Case four, with eight heated fins, likewise produces the greatest average liquid fraction values and completes the melting process in 850s. Additionally, when 6% nano-enhanced PCM was used instead of pure PCM, the melting process is accelerated by 28.57 percent.

Keywords: melting process, phase change material, GFEM/XFEM, fins, nusselt number

BACKGROUND INFORMATION

Energy storage technologies have risen in importance as a result of the unreliability of wind and solar energy sources, as well as their development in the efficiency and utilization of energy systems. Other PCM applications by [1] are of high importance in the industry due to the heat transfer mechanism of different PCM salts during phase change and of liquid salts. Also, using one storage module, the inclusion of PCM in solar cookers to extend usage time, and inclusion in a paint-drying system to recover exhaust heat are other important. [2] investigated thermal energy storage using curved-slab containers filled with phase change material and exposed to convective boundary conditions, taking into account heat transfer fluid flows between the containers. One of the results of improving the performance of the latent heat thermal energy storage system is that a significant quantity of storage capacity may be obtained at greater efficiency. [3] found that the temperature range is attributed to possible CO_2 emissions reductions that may be achieved by substituting cooling applications in residential and traditional heating. Diversifying energy supplies through the usage of suitable energy storage solutions and renewable energy sources, according to [4], are yardsticks for coming closer to energy sustainability.

[5] said that hot water tanks, which have a considerable influence on the tank's heat loss and internal thermal stratification, are a classic example of the most often utilized thermal energy storage. In research by [6] on the importance of electromagnetic nanomaterials coating processes with intricate chemical reactions, the nanoparticle concentration magnitude was discovered to be capable of decreasing with an increase in the chemical reaction. [7] investigated the effects of nanoparticles on the dynamics of a fluid in a 3D cubic with two rotating cylinders in the center of the enclosure exposed to Lorentz force, angular velocity under various circumstances, and mixed convection transport phenomena. It was determined that when angular velocity increased, cumulative energy and average temperature decreased. [8] explored mixed convection of phase change material (PCM) in a 3D cavity filled with a revolving cylinder when a temperature gradient occurred between the hot right vertical wall and the cold left vertical wall while the remaining walls were deemed adiabatic. Phase change materials (PCM) are one of the most effective and active topics of study in terms of long-term heat energy storage and thermal management due to their great qualities. It is worth noting that phase change materials (PCM) can be used in conjunction with solar collectors to store excess solar energy while also regulating the temperature of photovoltaic solar collectors.

Interactions between cell/tissue systems and nanoparticles are no longer a surprise. According to [9], there is a link between respiratory illness, environmental exposure, and nano-sized particles. [10] recently published the results of another investigation on the addition of multi-walled carbon nanoparticles to the dynamics of water within a vertical Cleveland Z-staggered cavity, which demonstrated that raising the Reynold number increases the inertial force. [11] revealed that an optimal mix of nanoparticles is another essential feature in increasing thermal transfer in an annular geometry comprising nanoliquids with variably heated borders. According to [12], adding nanoparticles to the base fluid reduces the strength of fluid flow and the rate of heat transmission. Due to the incorporation of nanoparticles in the host fluid of water, [13] discovered that shallow annular enclosures provide higher thermal performance with little entropy formation. According to [14], the great thermal conductivity of alumina nanoparticles permits the nanoparticles to effectively diffuse heat from the host base fluids via Brownian motion. Aluminum oxide is useful to improve the rheological and filtration properties of drilling fluid. Some hybrid nanoliquids flow owing to buoyancy across a non-uniformly heated annulus, as examined by [15], Oke [16], [17], [18], and [19]. It was discovered that the proper mix of nanoparticles is a critical criterion for improving heat transfer. [20] emphasized the significance of grapheme nanoparticles due to their monomolecular layer of carbon atoms that are bonded by their remarkable and unique structural, optical, and electrical capabilities.

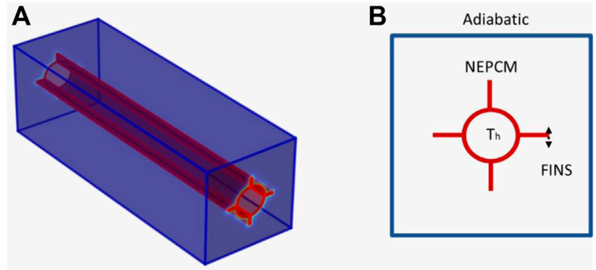

FIGURE 1 | Computational setup of LTESS **(A)** 3-D model **(B)** 2-D cross-section.

According to the findings of different studies on ternary-hybrid nanofluids by [21,22], [23], and [24], the viscosity and thermal conductivity of base fluids may be modified by the inclusion of nanoparticles. [25] investigated Darcy–Forchheimer nanoliquid convective flow in an odd-shaped cavity loaded with a multi-walled carbon nanotube-iron (II, III) oxide hybrid nanofluid when the walls are adiabatic and the internal and external cavity boundaries are isothermally is at low and high temperatures. In view of this, nothing is known on computational of alumina and n-octadecane melting performance inside energy storage system when the branched fins are two vertical but opposite fins, two horizontal but opposite fins, two vertical and two horizontal fins, and eight branched fins that are distributed. Research questions to be answered in this report are

1. At 500 s, what is the effect of the number of fins, liquid fraction, and Bejan number on the PCM melting process?
2. In the absence of volume fraction, what is the variations of temperature, liquid fraction, and Bejan number during the PCM melting process as time goes on?
3. At t = *500s*, how does increasing nanoparticle concentration, liquid fraction, and Bejan number affects alumina and n-octadecane melting performance in-side energy storage system?

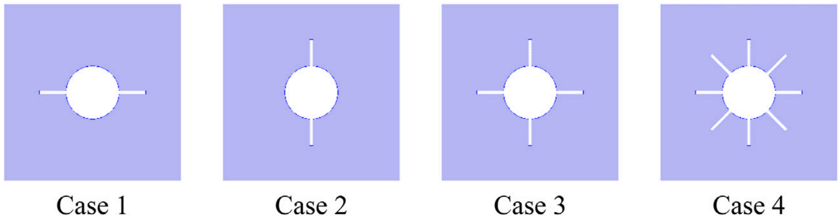

FIGURE 2 | Different cases of branched fins.

Table 1 | Properties of PCM and alumina.

Property	Al_2O_3	n-octadecane
$\rho\,[kg/m^3]$	3,970	770
$\beta\times 10^5\,[K^{-1}]$	0.85	91
$k\,[w/mK]$	40	0.157
$L\,[j/kg]$	–	242,9
Fusion [C]	–	28× 10^3
$\mu\times 10^3$[Pa.s]	–	3.79
$C_p\,[j/kgK]$	765	2,189

Sources [7] and [22].

4. What is the impact of fins number on the impact of fins number on liquid fraction, average Bejan number, average Nusselt number, and temperature distribution?

RESEARCH METHODOLOGY

The present computational model is shown in **Figure 1**. The heat transfer fluid is alumina and n-octadecane. Four distinct configurations of fins are modeled. The details of the four cases are shown in **Figure 2**. All fluids begin with a solidus temperature. The fined and cylinders were hot and adiabatic, respectively. The properties of nanoparticles and PCM are outlined in **Table 1**.

Problem Formulation

The GFEM technique was employed to simulate the transient flow that could be described as Newtonian and laminar. Boussinesq estimation was utilized to account for the gravitational force effect. The continuity (**Eq. 1**), momentum in x and y direction (**Eqs 2, 3**), and energy (**Eq. 4**) equations read [26] and [27].

$$\nabla\cdot\vec{V}=0 \tag{1}$$

$$\left(\frac{\partial v}{\partial t}+\vec{V}\cdot\nabla v\right)=vC\frac{(\lambda-1)^2}{\varepsilon+\lambda^3}+\frac{1}{\rho_{nf}}\left(-\nabla P+\mu_{nf}\nabla^2 v\right)+\frac{1}{\rho_{nf}}(\rho\beta)_{nf}g\left(T-T_{ref}\right) \tag{2}$$

$$\frac{\partial u}{\partial t}+\vec{V}\cdot\nabla u=uC\frac{(\lambda-1)^2}{\varepsilon+\lambda^3}+\frac{1}{\rho_{nf}}\left(-\nabla P+\mu_{nf}\nabla^2 u\right) \tag{3}$$

$$\left(\rho C_p\right)_{nf}\frac{\partial(\rho L\lambda)_{nf}}{\partial t}+\left(\rho C_p\right)_{nf}\frac{\partial T}{\partial t}-k_{nf}\nabla^2 T=-\left(\rho C_p\right)_{nf}\vec{V}\cdot\nabla T \tag{4}$$

The boundary conditions associated with **Eqs 1–4** for the inner hot wall

$$U=V=0,\quad \theta=1 \tag{5}$$

For the outer wall

$$U=V=0,\ \frac{\partial\theta}{\partial X}=0 \tag{6}$$

We considered $\varepsilon=10^{-3}, C=10^5$. A single-phase model was used to predict attributes Refs. [16 - 17]

$$\begin{aligned}&\left(\rho C_p\right)_f^{-1}\left(\rho C_p\right)_{nf}=(1-\phi)+\phi\left(\rho C_p\right)_s\left(\rho C_p\right)_f^{-1},\\&\rho_{nf}=\phi\rho_s+\rho_f(1-\phi),\ \mu_{nf}=\frac{\mu_f}{(1-\phi)^{2.5}}\\&(\rho\beta)_{nf}=\phi(\rho\beta)_s+(1-\phi)(\rho\beta)_f,\ (\rho L)_f=\frac{(\rho L)_{nf}}{(1-\phi)},\\&k_{nf}=\frac{2k_f+2\phi\left(k_s-k_f\right)+k_p}{k_p-\phi\left(k_s-k_f\right)+2k_f}k_f\end{aligned} \tag{7}$$

Enthalpy

The specific heat capacity of the PCM changes significantly with its phase. The specific enthalpy of the PCM is thus determined as a function of its temperature by [28] as

$$h=h_{ref}+\int_{T_{ret}}^{T}\left(C_p\right)_{nf}dT \tag{8}$$

Liquid fraction is introduced as

$$\lambda=\begin{cases}1 & T\le T_l\\ \dfrac{T-T_s}{T_l-T_s} & T_s\le T\le T_l,\ H_e=h+\lambda L\\ 0 & T\le T_s\end{cases} \tag{9}$$

The formula of $S_{gen,\,total}$, $S_{gen,\,th}$, $S_{gen,\,f}$ *and* $S_{gen,\,m}$ by [29]

$$S_{gen,total}=S_{gen,th}+S_{gen,\,f}+S_{gen,\,m} \tag{10}$$

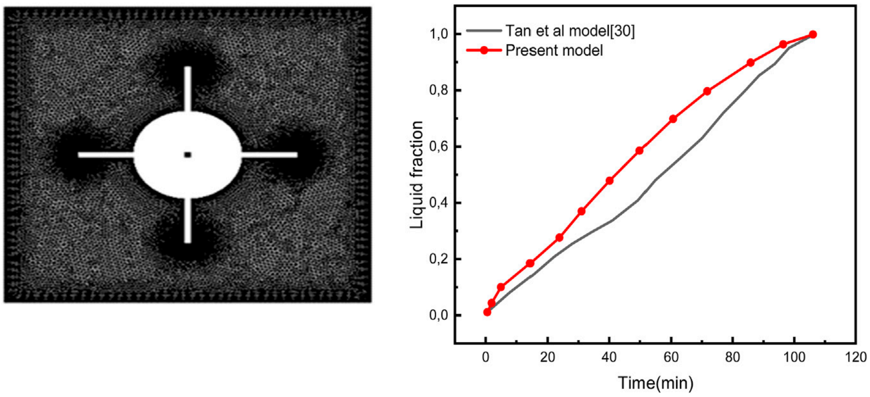

FIGURE 3 | Mesh grid and present model in comparison with [30].

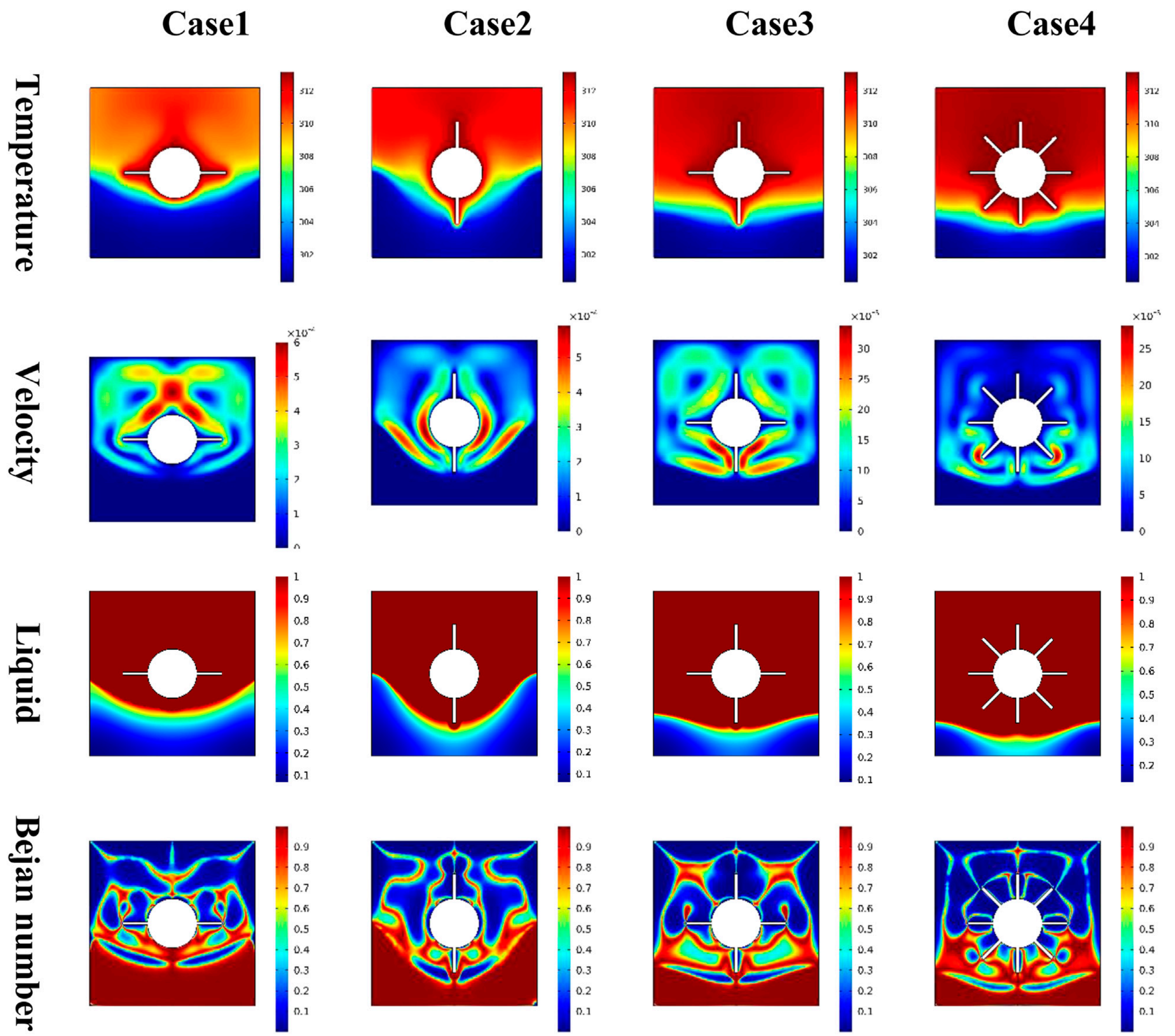

FIGURE 4 | Effect of the number of fins, liquid fraction, and Bejan number during the PCM melting process at 500 s.

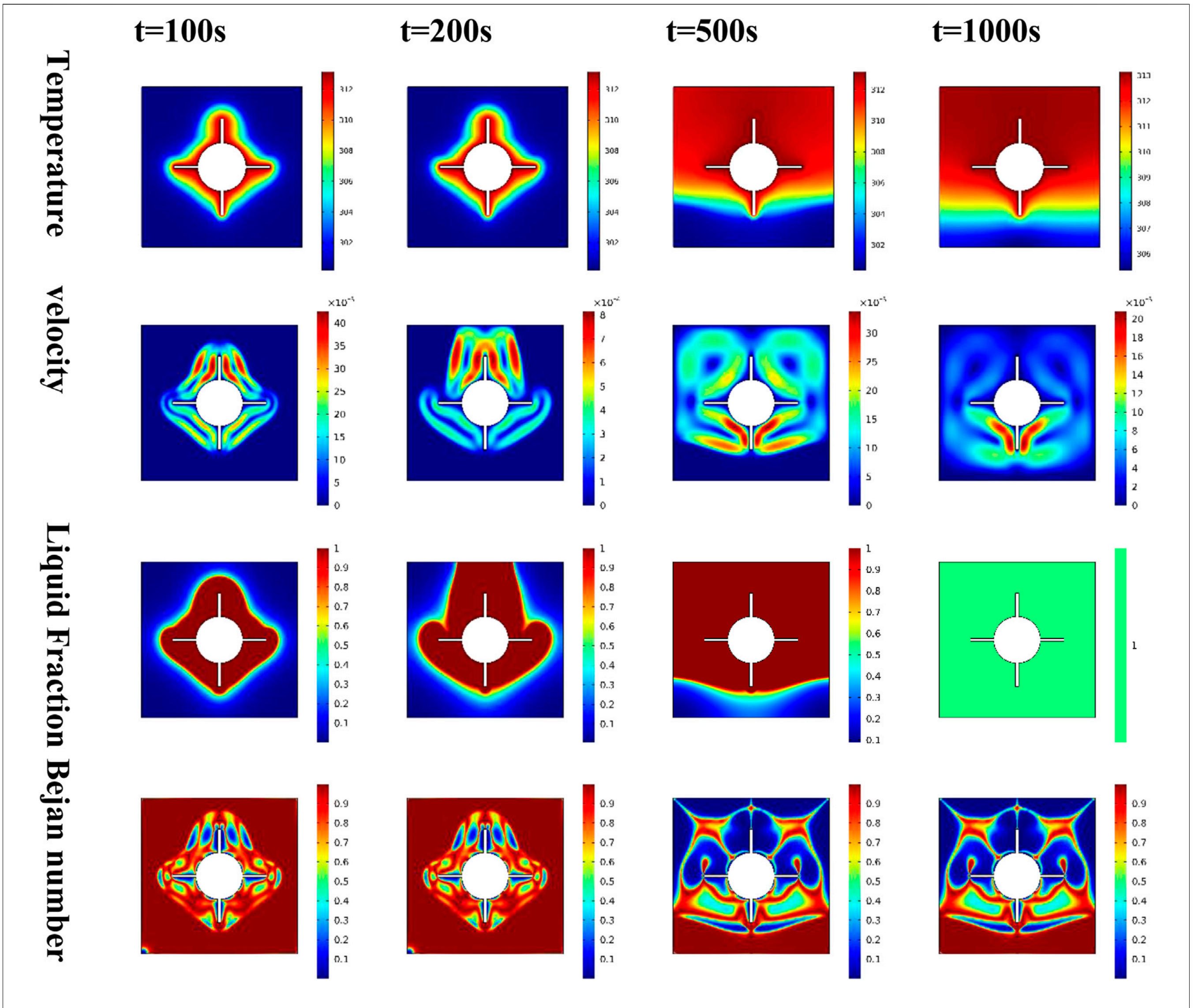

FIGURE 5 | Variations of temperature, liquid fraction, and Bejan number during. the PCM melting process as time goes on when $\phi = 0$.

$$S_{\text{gen,total}} = \frac{k_{nf}}{T^2}\left[\left(\frac{\partial T}{\partial x}\right)^2 + \left(\frac{\partial T}{\partial y}\right)^2\right] + \frac{\mu_{nf}}{T}\left\{2\left[\left(\frac{\partial u_x}{\partial x}\right)^2 + \left(\frac{\partial u_y}{\partial y}\right)^2\right] + \left(\frac{\partial u_x}{\partial y} + \frac{\partial u_y}{\partial x}\right)^2\right\} + N_\mu \frac{\sigma_{nf}}{\sigma_f} Ha^2 V^2$$

Where

$$N_\mu = \frac{\mu_f T_0}{k_f}\left(\frac{\alpha_f}{L(\Delta T)}\right)^2 \qquad (11)$$

Where $S_{\text{gen,th}}$ denotes the entropy production resulting from heat transfer irreversibility (HTI), $S_{\text{gen, f}}$ denotes the entropy production resulting from fluid friction irreversibility (FFI), and $S_{\text{gen, m}}$ denotes the entropy production resulting from magnetic field impacts. And consequently the mean Bejan numbers be determined as

$$B_e = \frac{S_{\text{gen, th}}}{S_{\text{gen, total}}} \qquad (12)$$

GFEM Approach

The transformed coupled **Eqs 1–4**, which comprise both the motion and heat transport processes as well as the requisite boundary conditions, are handled using the Galerkin Finite Element Method. First, on a non-uniform structural grid, the weak forms of the governing equations are presented and discretized. After that, mathematical software is used to model the outcomes and gives a detailed description of the procedure. It is crucial to keep in mind that the governing equations and their related constraints were solved by employing the Galerkin finite element technique. The programming environment is divided into triangle-shaped sections. Triangular Lagrange finite elements of various

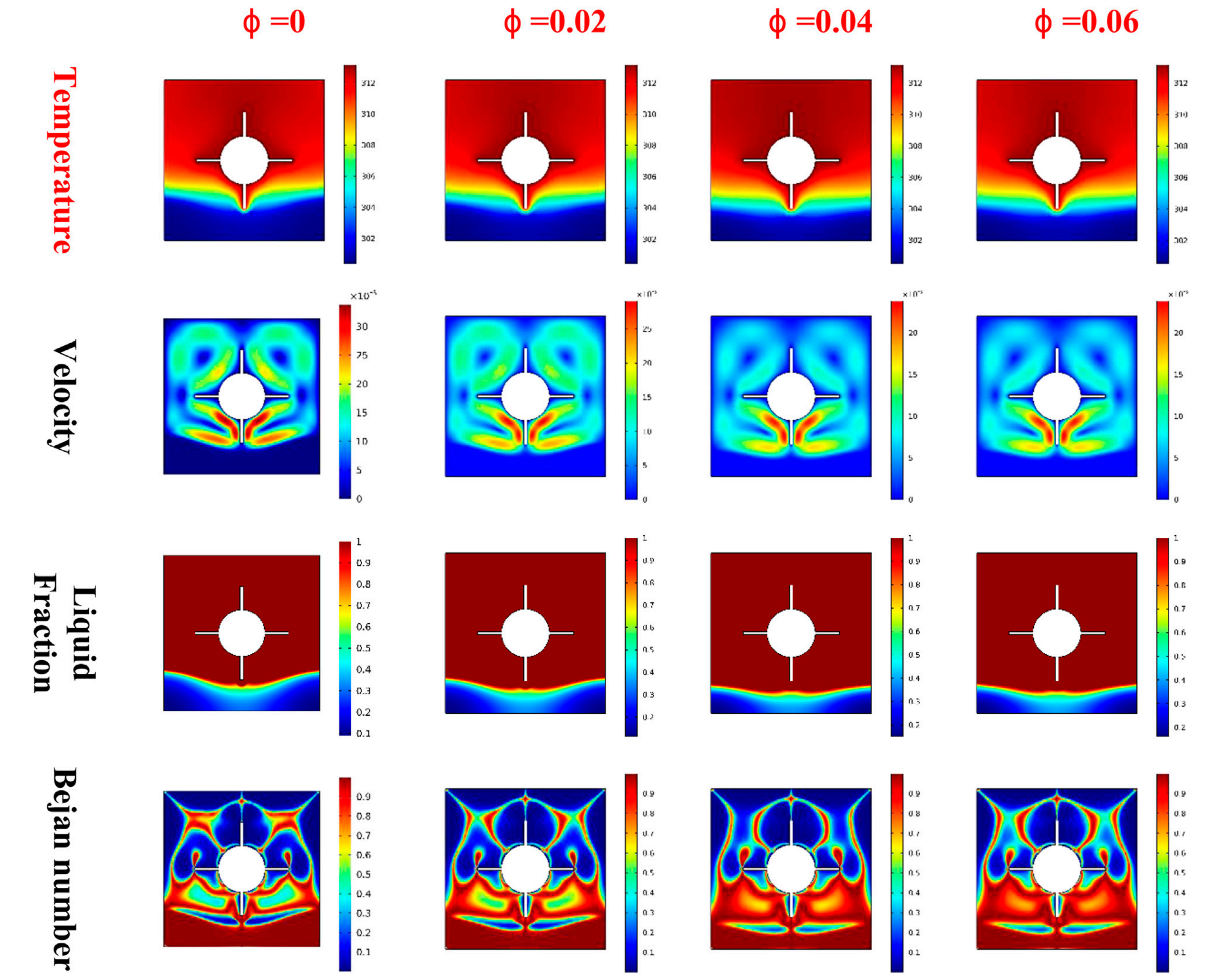

FIGURE 6 | Effect of nanoparticle concentration, liquid fraction, and Bejan number. during the PCM melting process at t = *500s*.

orders are employed on all the flow variables within the computational domain. By substituting the governing equations for the approximations, the residue is obtained.

$$\left|\frac{\Gamma^{i+1} - \Gamma^{i}}{\Gamma^{i}}\right| \leq 10^{-6} \tag{13}$$

Finally, using further numerical findings from [30], the validation of the current code is produced and illustrated in **Figure 3**. Based on this graph, we may be confident in our findings.

RESULTS AND DISCUSSION

The findings of studying the melting impacts on the motion of a suspension containing phase change material (PCM) are depicted and analyzed in this section. In this case, the heat transfer fluid is alumina and n-octadecane, and the motion area is a square tube with cross-section wings. For different heating scenarios, The isotherms lines, streamlines, Bejan number, and molten liquid of several cylinders are explored, including cylinders with two horizontal fins, cylinders with two vertical fins, cylinders with four fins, and cylinders with eight heated wings. Temporal Variations between 100 and 1000 s are investigated, and the nanoparticles volume percentage values are considered between 0 and 8%. The mean values of the molten PCM, Bejan number Be_{avg}, and Nusselt number Nuavg versus the progression of time are graphically displayed over a broad range of the studied parameters to offer a complete examination. The condition of the completely melted ($\beta = 1$) may also be utilized to stop the calculations. For different scenarios of inner heating, **Figure 4** shows the isotherms lines, streamlines, Bejan number, and molten PCM percentage. It should be noticed that the temperature

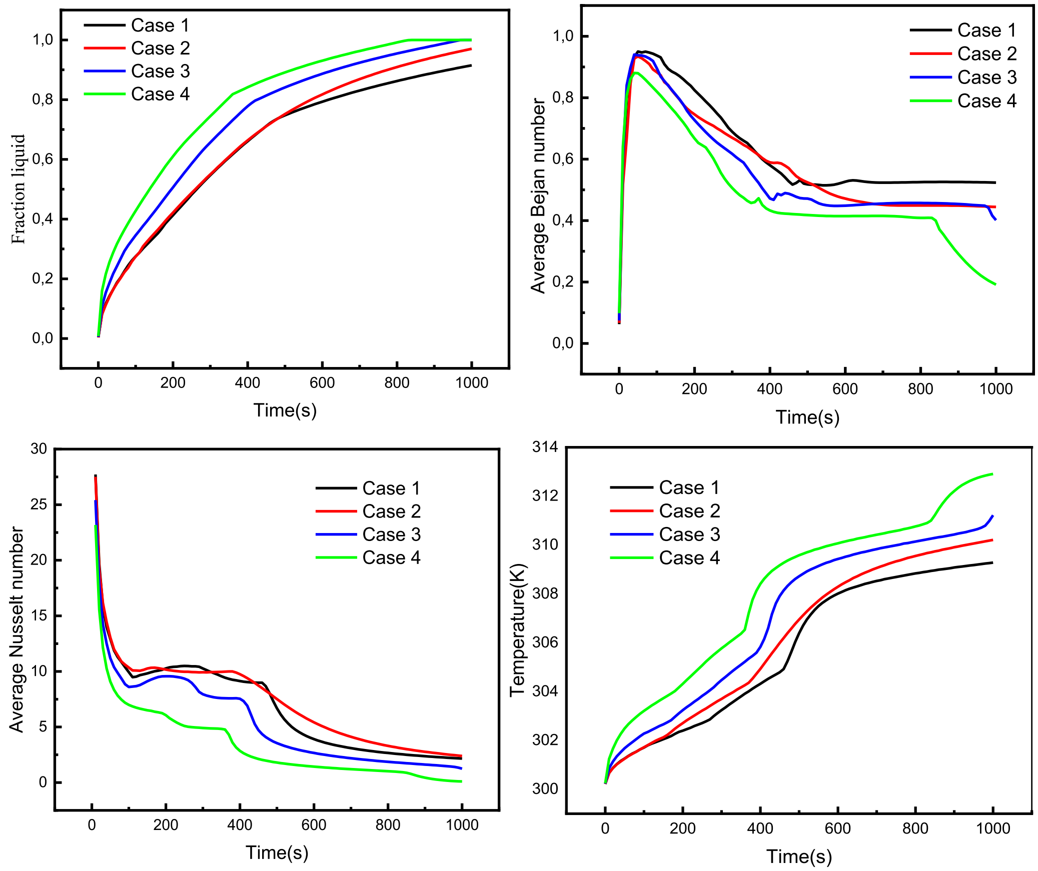

FIGURE 7 | The impact of fins number on liquid fraction, Average Bejan number, Average Nusselt number, and temperature distribution.

characteristics are focused around the fins in all instances, indicating a cold area around the outer cubic lowest. Case 4 (eight wings) had the highest temperature distributions, indicating a reduction in the above-mentioned cold area at the lowest.

It has also been noted that as the number of fins increases, the temperature differences decrease, so the temperature drop and thermal performance rate decrease. In addition, when the number of fins is improved, the velocity values clearly decrease. Physically, increasing the number of fins increases the complexity of the motion region, which increases motion resistance. Simultaneously, the characteristics of the Bejan number reveal that increasing the number of heated fins diminishes temperature gradients, and therefore fluid friction irreversibility takes over. In addition, the melting area appears in the top half of the area for all of the variables investigated, and the number of heated wings increases the volume of the melting zone. **Figure 5** depicts the characteristics of isotherms lines, streamlines, Be number, and mol-ten PCM percentage as time passes. Case 3 is employed in these calculations, using an inner cylinder with four wings. The findings showed that at the start of the computations (short time values), isotherms lines, streamlines, and Bejan number distributions occur around the inner heated zone, suggesting a non-active area towards the outer limits. The liquid begins to convey and disperse the temperature across the area as time passes. As a result, a suitable thermal domain with a greater velocity percentage towards the lowest of the outer borders is produced at time = 600. Furthermore, when comparing the fluid friction irreversibility to the heat transmission irreversibility, the higher the time value, the greater the dominance of the fluid friction irreversibility at the bottom. When the time values grow, the mushy zone appears across the whole flow domain.

Figure 6 depicts the isotherms lines, streamlines, Bejan number, and liquid fraction distributions as a function of the volume fraction parameter. In this situation, inner heated cylinders with four wings are employed. Due to the rise in the viscosity of the mixture, a poor convective transport is seen at higher values of. The data show that as it expands, the velocity and temperature gradients decrease. At low values of, the Be number occurs around the fins rather than the bottom borders. On the contrary, increasing increases the mushy zone

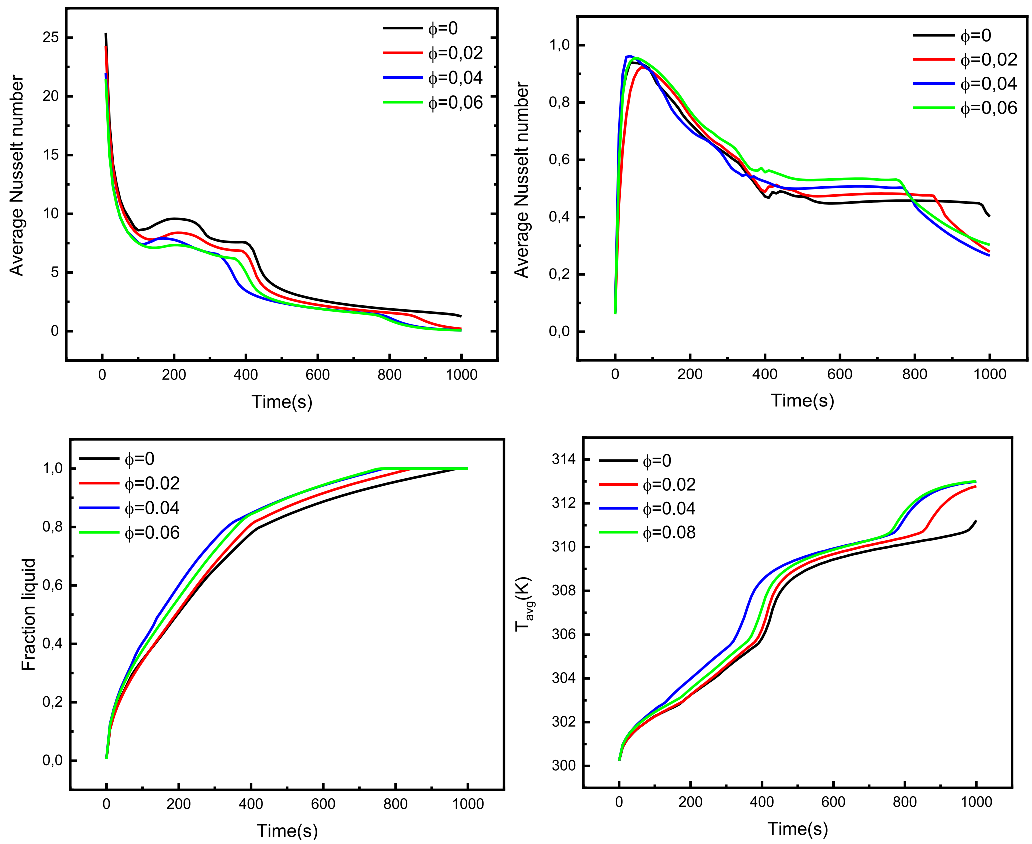

FIGURE 8 | The impact of nanoparticles concentration on molten liquid, Average Nusselt number (Nu_{avg}) and Average Nusselt number Average Nusselt number (Be_{avg}).

inside the motion region until the circumstances are entirely melted at 0.04. **Figure 7** and **Figure 8** show the mean molten PCM rate, Be^{avg}, and Nu_{avg} profiles as a function of the heated wings number, duration parameter, and concentration parameter.

The findings indicated that example 4, which assumes eight heated fins, had the highest β values. However, the Be_{avg} and $_{Nuavg}$ values decline when the number of heated wings increases. Furthermore, the average heat transfer rate decreases when the temperature gradients reduce. Furthermore, greater values of cause the irreversibility of heat transmission to take precedence over the irreversibility of fluid friction. Finally, increasing the nanoparticles concentration improves the mushy zone, increasing the β.

CONCLUSION

The current research numerically investigated the influence of inserting different numbers of branched fins inside energy storage system on the melting process of alumina and n-octadecane. Based on the number of heated fins, four instances were considered. The shaky scenario was taken into account, and fully melted situations were anticipated. The governing system was solved using the finite element technique (GFEM) and the Poisson pressure equation. The following are some of the most important findings:

1. As the heated fins increase due to the enhancement in the buoyancy-convective situation, the temperature, velocity, and Bejan number distributions increase. In scenario 4, the melted area was also regulated throughout the majority of the flow domain.
2. Isotherms lines, streamlines, and molten PCM occur around the inner heated forms at short values of time, whereas as time passes, a nice isothermal and melted motion domain was produced.
3. As it rises, the dynamic viscosity of the mixture increases, and as a result, the velocity of the mixture decreases.
4. When compared to heat transmission irreversibility, the irreversibility owing to fluid friction becomes more dominant with time.

5. Case four, with eight heated fins, likewise produces the greatest average liquid fraction values and completes the melting process in 850 s.
6. When 6% nano-enhanced PCM was used instead of pure PCM, the melting process was found to accelerate by 28.57 percent.

DATA AVAILABILITY STATEMENT

The original contributions presented in the study are included in the article/supplementary material, further inquiries can be directed to the corresponding author.

AUTHOR CONTRIBUTIONS

All authors listed have made a substantial, direct, and intellectual contribution to the work and approved it for publication.

FUNDING

Authors extend their appreciation to the Deanship of Scientific Research at King Khalid University for funding this work through research group under grant number R.G.P.2/224/43. The authors would like to thank the Deanship of Scientific Research at Umm Al-Qura University for supporting this work by Grant Code: (22UQU4331317DSR21).

REFERENCES

1. Zalba B., Marı´n JM, Cabeza L. F., Mehling H. Review on thermal Energy Storage with Phase Change: Materials, Heat Transfer Analysis and Applications. *Appl Therm Eng* (2003) 23(3):251–83. doi:10.1016/s1359-4311(02)00192-8
2. Koizumi H, Jin Y. Performance Enhancement of a Latent Heat thermal Energy Storage System Using Curved-Slab Containers. *Appl Therm Eng* (2012) 37: 145–53. doi:10.1016/j.applthermaleng.2011.11.009
3. Pereira da Cunha J, Eames P. Thermal Energy Storage for Low and Medium Temperature Applications Using Phase Change Materials – A Review. *Appl Energy* (2016) 177:227–38. doi:10.1016/j.apenergy.2016.05.097
4. Dinçer I, Rosen M A. Renewable Energy Systems with Thermal Energy Storage. *Therm Energy Storage* (2021) 521–55. doi:10.1002/9781119713173.ch7
5. Cabeza L. F. Advances in Thermal Energy Storage Systems: Methods and Applications. *Advanc in Therm Energy Storage Systems* (2021) 37–54. doi:10.1016/b978-0-12-819885-8.00002-4
6. Shahid A., Bhatti M. M., Anwar Bég O., Animasaun I. L., Javid K. Spectral Computation of Reactive Bi-directional Hydromagnetic Non-Newtonian Convection Flow from a Stretching Upper Parabolic Surface in Non-Darcyporous Medium. *Int J Mod Phys B* (2021) 35(29):2150294. doi:10.1142/s0217979221502945
7. Abderrahmane A., Hatami M., Younis O., Mourad A. Effect of Double Rotating Cylinders on the MHD Mixed Convection and Entropy Generation of a 3D Cubic Enclosure Filled by Nano-PCM. *Eur Phys J Spec Top.* (2022). doi:10.1140/epjs/s11734-022-00586-7
8. Al-Kouz W., Aissa A., Uma Devi S., Prakash M., Kolsi L., Moria H., et al.Effect of a Rotating cylinder on the 3D MHD Mixed Convection in a Phase Change Material Filled Cubic Enclosure. *Sustain Energy Technologies and Assessments* (2022) 51:101879. doi:10.1016/j.seta.2021.101879
9. Tortorella S., Karagiannis T. C. The Significance of Nanoparticles in Medicine and Their Potential Application in Asthma. In: N Maulik T Karagiannis, editors. *Molecular Mechanisms and Physiology of Disease*. New York, NY: Springer (2014). p. 247–75. doi:10.1007/978-1-4939-0706-9_10
10. Rasool G., Saeed A. M., Lare A. I., Abderrahmane A., Guedri K., Vaidya H., et al.Darcy-Forchheimer Flow of Water Conveying Multi-Walled Carbon Nanoparticles through a Vertical cleveland Z-Staggered Cavity Subject to Entropy Generation. *Micromachines* (2022) 13:744. doi:10.3390/mi13050744
11. Reddy N. K., Swamy H. A. K., Sankar M. Buoyant Convective Flow of Different Hybrid Nanoliquids in a Non-uniformly Heated Annulus. *Eur Phys J Spec Top.* (2021) 230(5):1213–25. doi:10.1140/epjs/s11734-021-00034-y
12. Sankar M., Swamy H. A. K., Do Y., Altmeyer S. Thermal Effects of Nonuniform Heating in a Nanofluid-filled Annulus: Buoyant Transport versus Entropy Generation. *Heat Trans* (2022) 51(1):1062–91. doi:10.1002/htj.22342
13. Swamy H. A. K., Sankar M., Reddy N. K. Analysis of Entropy Generation and Energy Transport of Cu-Water Nanoliquid in a Tilted Vertical Porous Annulus. *Int J Appl Comput Math* (2022) 8(1):1–23. doi:10.1007/s40819-021-01207-y
14. Song Y.-Q., Obideyi B. D., Shah N. A., Animasaun I. L., Mahrous Y. M., Chung J. D. Significance of Haphazard Motion and Thermal Migration of Alumina and Copper Nanoparticles across the Dynamics of Water and Ethylene Glycol on a Convectively Heated Surface. *Case Studi Thermal Engineering* (2021) 26: 101050. doi:10.1016/j.csite.2021.101050
15. Keerthi Reddy N., Sankar M. Buoyant Convective Transport of Nanofluids in a Non-uniformly Heated Annulus. *J Phys Conf. Ser*(2020) 1597(1):012055. doi:10.1088/1742-6596/1597/1/012055
16. Oke A. S. Heat and Mass Transfer in 3D MHD Flow of EG-Based Ternary Hybrid Nanofluid over a Rotating Surface. *Arab J Sci Eng* (2022) 1-17. in-press. doi:10.1007/s13369-022-06838-x
17. Oke A. S., Mutuku W. N. Significance of Viscous Dissipation on MHD Eyring-Powell Flow Past a Convectively Heated Stretching Sheet. *Pramana J Phys* (2021) 95(4):1–7. doi:10.1007/s12043-021-02237-3
18. Reddy N. K., Swamy H. A., Sankar M. Buoyant Convective Flow of Different Hybrid Nanoliquids in a Non-uniformly Heated Annulus. *European Physical Journal Special Topics* (2021) 230(5):1213–25. doi:10.1140/epjs/s11734-021-00034-y
19. Mebarek-Oudina F., Keerthi Reddy N., Sankar M. Heat Source Location Effects on Buoyant Convection of Nanofluids in an Annulus. In: *Advances in Fluid Dynamics*. Singapore: Springer (2021). p. 923–37. doi:10.1007/978-981-15-4308-1_70
20. Sharma R., Raju C. S., Animasaun I. L., Santhosh H. B., Mishra M. K. Insight into the Significance of Joule Dissipation, thermal Jump and Partial Slip: Dynamics of Unsteady Ethelene Glycol Conveying Graphene Nanoparticles through Porous Medium. *Nonlinear Engineering* (2021) 10(1):16–27. doi:10.1515/nleng-2021-0002
21. Animasaun I. L., Yook S.-J., Muhammad T., Mathew A. Dynamics of Ternary-Hybrid Nanofluid Subject to Magnetic Flux Density and Heat Source or Sink on a Convectively Heated Surface. *Surfaces and Interfaces* (2022) 28:101654. doi:10.1016/j.surfin.2021.101654
22. Animasaun I. L., Shah N. A., Wakif A., Mahanthesh B., Sivaraj R., Koriko O. K. *Ratio of Momentum Diffusivity to Thermal Diffusivity: Introduction, Meta-Analysis, and Scrutinization*. New York: Chapman and Hall/CRC (2022). ISBN-13: 978-1032108520, ISBN-10: 1032108525, ISBN9781003217374.
23. Saleem S., Animasaun I. L., Yook S.-J., Al-Mdallal Q. M., Shah N. A., Faisal M. Insight into the Motion of Water Conveying Three Kinds of Nanoparticles Shapes on a Horizontal Surface: Significance of Thermo-Migration and Brownian Motion. *Surfaces and Interfaces* (2022) 30:101854. doi:10.1016/j.surfin.2022.101854
24. Cao W., I.L. A., Yook S.-J., V.A. O., Ji X. Simulation of the Dynamics of Colloidal Mixture of Water with Various Nanoparticles at Different Levels of Partial Slip: Ternary-Hybrid Nanofluid. *International Communicatioin Heat and Mass Transfer* (2022) 135:106069. doi:10.1016/j.icheatmasstransfer.2022.106069
25. Al-Kouz W, Aissa A, Koulali A, Jamshed W, Moria H, Nisar KS, et al.MHD Darcy-Forchheimer Nanofluid Flow and Entropy Optimization in an Odd-Shaped Enclosure Filled with a (MWCNT-Fe3O4/water) Using Galerkin Finite Element Analysis. *Sci Rep* (2021) 11(1):22635–15. doi:10.1038/s41598-021-02047-y
26. Sheikholeslami M., Jafaryar M., Shafee A., Li Z. Hydrothermal and Second Law Behavior for Charging of NEPCM in a Two Dimensional thermal

Storage Unit. *Chinese Journal of Physics* (2019) 58:244–52. doi:10.1016/j.cjph.2019.02.001

27. Mourad A., Aissa A., Said Z., Younis O., Iqbal M., Alazzam A. Recent Advances on the Applications of Phase Change Materials for Solar Collectors, Practical Limitations, and Challenges: A Critical Review. *Journal Energrgy Storage* (2022) 49:104186. doi:10.1016/j.est.2022.104186
28. Bouzennada T., Mechighel F., Filali A., Ghachem K., Kolsi L. Numerical Investigation of Heat Transfer and Melting Process in a PCM Capsule: Effects of Inner Tube Position and Stefan Number. *Case Stud Thermal Engineering* (2021) 27:101306. doi:10.1016/j.csite.2021.101306
29. Abderrahmane A. MHD Hybrid Nanofluid Mixed Convection Heat Transfer and Entropy Generation in a 3-D Triangular Porous Cavity with Zigzag Wall and Rotating Cylinder. *Mathematics* (2022) 10(5):769. doi:10.3390/math10050769
30. Tan F. L., Hosseinizadeh S. F., Khodadadi J. M., Fan L. Experimental and Computational Study of Constrained Melting of Phase Change Materials (PCM) inside a Spherical Capsule. *Int J Heat and Mass Transfer* (2009) 52: 3464–72. doi:10.1016/j.ijheatmasstransfer.2009.02.043

Conflict of Interest: The authors declare that the research was conducted in the absence of any commercial or financial relationships that could be construed as a potential conflict of interest.

Publisher's Note: All claims expressed in this article are solely those of the authors and do not necessarily represent those of their affiliated organizations, or those of the publisher, the editors and the reviewers. Any product that may be evaluated in this article, or claim that may be made by its manufacturer, is not guaranteed or endorsed by the publisher.

NOMENCLATURE

$C_p\,(J/kg.K)$ Heat capacity

$k\,(W/m.K)$ Thermal conductivity

$L_f\,(KJ/Kg)$ Latent heat coefficient

$\mathbf{P}$ $\mathbf{(kg/m.s^2)}$ Pressure

$\mathbf{g}$ Acceleration vector of gravity

h_{ref} Reference sensible enthalpy

$T_m\,(K)$ Fusion temperature

$\triangle\mathbf{H}$ **(J/kg)** Latent heat content

Abbreviations

PCM Phase change material

2D Two-dimensional

C Mushy zone morphology constant

LHTES Latent heat thermal energy storage

Greek

$\rho\,(\mathrm{Kg}/m^3)$ Density

μ $(\mathrm{Pa}\cdot\mathrm{s})$ Dynamic viscosity

$\alpha\,(\mathrm{m^2/s})$ Thermal diffusivity